Letter to the editor

Lower bound limit analysis by quadrilateral elements

Chunguang Li [a,*], Cong Sun [c], Cuihua Li [a,b], Hong Zheng [a]

[a] State Key Laboratory of Geomechanics and Geotechnical Engineering, Institute of Rock and Soil Mechanics, Chinese Academy of Sciences, Wuhan 430071, China
[b] Hubei Water Resources Technical College, Wuhan 430202, China
[c] Wuhan municipal construction group Co., Ltd., 430023, China

ARTICLE INFO

ABSTRACT

This paper presents a quadrilateral element formulation of lower bound theorem. The formulation uses a four-noded quadrilateral element. The weak form of the equilibrium equations is performed to linearize the equilibrium equations. By Green's theorem, the integral over quadrilateral element are transformed into boundary integral over the element boundary. The major advantage of using quadrilateral element, rather than triangular element, is that more accurate lower bound can be obtained with the same element size.

Two numerical examples are given to illustrate the capability of the new method for computing lower bound. The accuracy of the quadrilateral element formulation is compared with that of three-noded triangular element formulation in detail.

© 2016 Elsevier B.V. All rights reserved.

1. Introduction

As an effective method to estimate the ultimate bearing capacity for structures, lower- and upper-bound limit analysis have been extensively used in the past in a wide variety of problems, such as tunnels [1,2], slopes [3,4], foundations [5,6], anchors [7,8], braced excavations [9,10]. Accurate assessment of the stability of those structures is an important task.

To make the 'gap' between the upper- and lower-bound limit loads smaller, some adaptive meshing strategies have been developed, for example, based on the deformations and on the slack in the yield condition, Christiansen et al. presented a strategy for automatic mesh refinement in limit analysis [11]. Lyamin et al. adapted the approach of Borges and developed an adaptive remeshing procedure for lower bound limit analysis [12]. Based on elemental and edge contributions to the bound gap, Munoz et al. construct a new error estimate employed in an adaptive remeshing strategy which is able to reproduce fan-type mesh patterns around points with discontinuous surface loading [13].

In displacement finite-element analysis, triangular elements and quadrilateral elements are fundamentally different. We are aware of that general quadrilateral elements are very frequently encountered in two-dimensional analyses and linear triangular element is less accurate compared to linear quadrilateral element, but in finite-element limit analysis, three-node triangular element is employed exclusively for two-dimensional problems, since this leads to an optimization problem with linear constraints.

In this paper, we extend the quadrilateral element to lower- and upper-bound limit analysis based on the weak form of the equilibrium equations. It is also shown that quadrilateral element is not only more accurate than triangular element, but it converges faster than triangular element as the mesh is refined.

---

* Corresponding author.
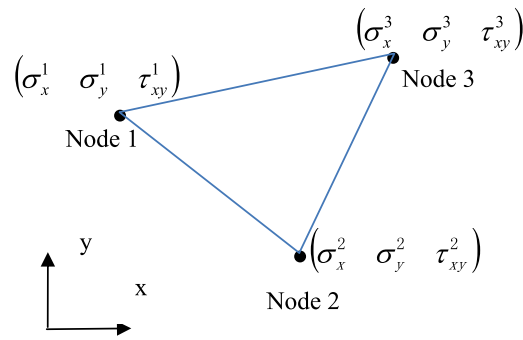E-mail address: cgli@whrsm.ac.cn (C. Li).

Fig. 1. Three-node linear stress triangle for lower bound limit analysis.

2. Brief review of limit analysis

2.1. Lower bound theorem

Consider a body of volume V with surface area S, if the state stress inside V, σ_{ij}, satisfies equilibrium equations with body forces b_i and the surface tractions T_i acting along the surface S_T, and does not violate the yield criterion $f(\sigma_{ij})$ at any point, then collapse does not occur. That is to say, the applied load is definitely less than or at most equal to the true collapse load. This problem can be reformulated to an optimization problem of the form

$$
\text{Max} : \lambda
$$
$$
\text{S.t.} \begin{cases} \sigma_{ij,j} + \lambda b_i = 0 & \text{(in } V) \\ f(\sigma_{ij}) \leq 0 & \text{(in } V) \\ \sigma_{ij} n_j = \lambda \overline{T_i} & \text{(on } S_T). \end{cases}
\tag{1}
$$

In this paper, the Mohr–Coulomb yield criterion is chosen to model the plastic flow in soils.

2.2. Discrete formulation of the lower bound theorem

Based on a linear three-node triangle, with the unknowns being the stresses at each node, shown in Fig. 1, the variation of the stress throughout each element is linear and each node is associated with 3 unknown stresses σ_X, σ_Y and τ_{XY}, Each stress varies through an element according to

$$
\sigma_X = \sum_{i=1}^{3} N_i \sigma_x^i, \qquad \sigma_Y = \sum_{i=1}^{3} N_i \sigma_y^i, \qquad \tau_{XY} = \sum_{i=1}^{3} N_i \tau_{xy}^i
\tag{2}
$$

where σ_x^i, σ_y^i and τ_{xy}^i are the nodal stresses and N_i, are linear shape functions. These shape functions are

$$
N_i = \frac{1}{2A}(a_i + b_i x + c_i y)
\tag{3}
$$

where

$$
a_i = x_j y_k - x_k y_j, \qquad b_i = y_j - y_k, \qquad c_i = -x_j + x_k
\tag{4}
$$

i, j, k are counterclockwise sequence numbers for the three nodes, respectively, and A is the element area.

The lower bound problem can then be stated as a linear programming problem of the form

$$
\text{Max} : \lambda
$$
$$
\text{S.t.} \begin{cases} [A_1]\{\sigma\} = \lambda\{b_1\} \\ [A_2]\{\sigma\} \leq \{b_2\} \end{cases}
\tag{5}
$$

in which $\{\sigma\}$ is a global vector of unknown nodal stresses, $[A_1]$ is a matrix of all equality constraints and $[A_2]$ is a matrix of yield constraints. The equality constraints include continuum and discontinuity equilibrium and stress boundary conditions, the inequalities represent the linearized yield conditions.

3. Quadrilateral elements for lower bound limit analysis

3.1. Stress approximation

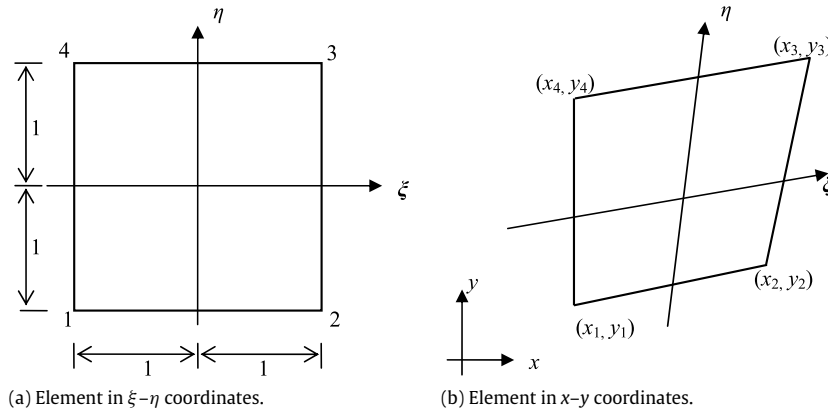A four-node two-dimensional quadrilateral is shown in Fig. 2.

(a) Element in ξ–η coordinates.   (b) Element in x–y coordinates.

Fig. 2. Isoparametric map for 4-node two-dimensional quadrilateral.

A finite element approximation for stresses is given by

$$\boldsymbol{\sigma}(\mathbf{x}) \approx \tilde{\boldsymbol{\sigma}} = \sum_{i=1}^{4} N_i(\mathbf{x})\boldsymbol{\sigma}^i \tag{6}$$

where $\boldsymbol{\sigma} = [\sigma_x, \sigma_y, \tau_{xy}]$ and N_i are element shape functions. Alternatively, in isoparametric form the expressions are given by

$$\boldsymbol{\sigma}(\boldsymbol{\xi}) \approx \tilde{\boldsymbol{\sigma}} = \sum_{i=1}^{4} N_i(\boldsymbol{\xi})\boldsymbol{\sigma}^i \tag{7a}$$

$$\mathbf{x}(\boldsymbol{\xi}) = \sum_{i=1}^{4} N_i(\boldsymbol{\xi})\mathbf{x}^i \tag{7b}$$

where $\mathbf{x}^i$ represent nodal coordinates and $\boldsymbol{\xi}$ are the parametric coordinates for each element.

The four shape functions are bilinear functions, given as

$$\begin{aligned}
N_1 &= \frac{1}{4}(1 - \xi)(1 - \eta) \\
N_2 &= \frac{1}{4}(1 + \xi)(1 - \eta) \\
N_3 &= \frac{1}{4}(1 + \xi)(1 + \eta) \\
N_4 &= \frac{1}{4}(1 - \xi)(1 + \eta).
\end{aligned} \tag{8}$$

Since $|\xi| \leq 1$ and $|\eta| \leq 1$,

$$N_i \geq 0, \quad i = 1\text{–}4 \tag{9}$$

is true.

Notice that

$$\sum_{i=1}^{4} N_i = 1, \tag{10}$$

which means that shape functions are partitions of unity.

3.2. Element equilibrium

The stress throughout each element must obey the following equations

$$\begin{aligned}
\frac{\partial \sigma_x}{\partial x} + \frac{\partial \tau_{xy}}{\partial y} &= 0 \\
\frac{\partial \tau_{xy}}{\partial x} + \frac{\partial \sigma_y}{\partial y} &= \gamma
\end{aligned} \tag{11}$$

where γ is the soil unit weight and tensile stresses are taken as positive.

Substituting (6) into (11) gives

$$\mathbf{B}^e_{eq}\boldsymbol{\sigma}^e = \mathbf{b}^e \tag{12}$$

where

$$\boldsymbol{\sigma}^e = \begin{bmatrix} \boldsymbol{\sigma}^1 & \boldsymbol{\sigma}^2 & \boldsymbol{\sigma}^3 & \boldsymbol{\sigma}^4 \end{bmatrix}^T \tag{13}$$

$$\mathbf{b}^e = \begin{bmatrix} 0 & \gamma \end{bmatrix}^T \tag{14}$$

$$\mathbf{B}^e_{eq} = \begin{bmatrix} \mathbf{B}^1 & \mathbf{B}^2 & \mathbf{B}^3 & \mathbf{B}^4 \end{bmatrix}. \tag{15}$$

$$\mathbf{B}^i = \begin{bmatrix} \dfrac{\partial N_i}{\partial x} & 0 & \dfrac{\partial N_i}{\partial y} \\ 0 & \dfrac{\partial N_i}{\partial y} & \dfrac{\partial N_i}{\partial x} \end{bmatrix}, \quad i = 1\text{–}4. \tag{16}$$

$$\begin{Bmatrix} \dfrac{\partial N_i}{\partial x} \\ \dfrac{\partial N_i}{\partial y} \end{Bmatrix} = [J]^{-1} \begin{Bmatrix} \dfrac{\partial N_i}{\partial \xi} \\ \dfrac{\partial N_i}{\partial \eta} \end{Bmatrix} \tag{17}$$

$$[J] = \begin{bmatrix} \dfrac{\partial N_1}{\partial \xi} & \dfrac{\partial N_2}{\partial \xi} & \dfrac{\partial N_3}{\partial \xi} & \dfrac{\partial N_4}{\partial \xi} \\ \dfrac{\partial N_1}{\partial \eta} & \dfrac{\partial N_2}{\partial \eta} & \dfrac{\partial N_3}{\partial \eta} & \dfrac{\partial N_4}{\partial \eta} \end{bmatrix} \begin{bmatrix} x_1 & y_1 \\ x_2 & y_2 \\ x_3 & y_3 \\ x_4 & y_4 \end{bmatrix}. \tag{18}$$

Unlike the element equilibrium for triangular element, Eq. (12) cannot be true everywhere in the element, since shape function is not a linear function of coordinates.

Fortunately, by integral over the element, Eq. (12) can be satisfied in an average sense (weak form),

$$\bar{\mathbf{B}}^e_{eq}\boldsymbol{\sigma}^e = \mathbf{b}^e \tag{19}$$

where

$$\bar{\mathbf{B}}^e_{eq} = \begin{bmatrix} \bar{\mathbf{B}}_1 & \bar{\mathbf{B}}_2 & \bar{\mathbf{B}}_3 & \bar{\mathbf{B}}_4 \end{bmatrix} \tag{20}$$

and

$$\bar{\mathbf{B}}_i = \frac{1}{A^e} \int_e \begin{bmatrix} \dfrac{\partial N_i}{\partial x} & 0 & \dfrac{\partial N_i}{\partial y} \\ 0 & \dfrac{\partial N_i}{\partial y} & \dfrac{\partial N_i}{\partial x} \end{bmatrix} dA, \quad i = 1\text{–}4. \tag{21}$$

Obviously, $\bar{\mathbf{B}}^e_{eq}$ is constant for element e.

By Green's theorem, Eq. (21) can be rewritten as

$$\bar{\mathbf{B}}_i = \frac{1}{A^e} \begin{bmatrix} \oint N_i dy & 0 & -\oint N_i dx \\ 0 & -\oint N_i dx & \oint N_i dy \end{bmatrix}. \tag{22}$$

By the linearity of N_i on boundary, we have

$$\begin{cases} \oint N_i dy = \dfrac{1}{2}(y_{i\,Mod4+1} - y_{(i-2)\,Mod4+1}) \\ \oint N_i dx = \dfrac{1}{2}(x_{i\,Mod4+1} - x_{(i-2)\,Mod4+1}) \end{cases} \tag{23}$$

in which *Mod* is the modulo operator.

3.3. Yield condition

For plane strain conditions, the Mohr–Coulomb yield criterion can be expressed as

$$f(\sigma_x, \sigma_y, \tau_{xy}) = \sqrt{(\sigma_x - \sigma_y)^2 + (2\tau_{xy})^2} + (\sigma_x + \sigma_y)\sin\varphi - 2c\cos\varphi \leq 0. \tag{24}$$

The Hessian matrix **H** of f is a square 3×3 matrix, arranged as follows:

$$\mathbf{H} = \frac{4\tau_{xy}^2}{\left[(\sigma_x - \sigma_y)^2 + (2\tau_{xy})^2\right]^{3/2}} \begin{bmatrix} 1 & -1 & -a \\ -1 & 1 & a \\ -a & a & a^2 \end{bmatrix} \tag{25}$$

where $a = \frac{\sigma_x - \sigma_y}{\tau_{xy}}$.

The eigenvalues of **H** are $4\left[(\sigma_x - \sigma_y)^2 + 2\tau_{xy}^2\right] / \left[(\sigma_x - \sigma_y)^2 + (2\tau_{xy})^2\right]^{3/2}$ and 0 (repeated). Since all eigenvalues of **H** are greater than or equal to 0, **H** is a positive-semidefinite matrix, and the Mohr–Coulomb yield function f is a convex function. From the view of Mohr–Coulomb yield surface in $\sigma_x - \sigma_y - \tau_{xy}$ space, as shown in Fig. 3, we know that the Mohr–Coulomb yield surface is a cone and

$$c(\boldsymbol{\sigma}) = \left\{ (\boldsymbol{\sigma}) | f(\boldsymbol{\sigma}) \leq 0, \boldsymbol{\sigma} \in R^3 \right\} \tag{26}$$

is a convex set.

For any point **x** in a quadrilateral element, the stress $\boldsymbol{\sigma}$ at point **x** in element e can be represented by

$$\boldsymbol{\sigma}(\mathbf{x}) = \sum_{i=1}^{4} N_i(\mathbf{x})\boldsymbol{\sigma}^i, \quad \mathbf{x} \in e. \tag{27}$$

Since $\sum_{i=1}^{4} N_i = 1$ and $N_i \geq 0$, $\boldsymbol{\sigma}(\mathbf{x})$ is a convex combination of $\boldsymbol{\sigma}^1, \boldsymbol{\sigma}^2, \boldsymbol{\sigma}^3$ and $\boldsymbol{\sigma}^4$. Provided

$$f(\boldsymbol{\sigma}^i) \leq 0, \quad i = 1\text{–}4 \tag{28}$$

this means that $\boldsymbol{\sigma}^i (i = 1\text{–}4)$ are all in the convex set $c(\boldsymbol{\sigma})$, therefore $\boldsymbol{\sigma}(\mathbf{x})$ is also in the set $c(\boldsymbol{\sigma})$ for any point **x** in the element e, that is to say,

$$f(\boldsymbol{\sigma}(\mathbf{x})) \leq 0, \quad \forall \mathbf{x} \in e. \tag{29}$$

In order that the yield condition is satisfied throughout the element, it is sufficient to enforce this yield constraint at each nodal point of each quadrilateral element. Using the linear approximation of the yield surface [14], the stresses at all nodes in the finite element model must satisfy the following inequality

$$[A_2]\{\sigma\} \leq \{b_2\}. \tag{30}$$

4. Finite element formulation of the lower bound method

With the Mohr–Coulomb yield function approximated by an interior polygon, along with discontinuities equilibrium and boundary conditions [14], the discrete form of the lower bound theory can be expressed as:

$$\begin{aligned} \max\ &: [c]^T \{\sigma\} \\ \text{s.t.}\ &: [A_1]\{\sigma\} = b_1 \\ &\quad [A_2]\{\sigma\} \leq b_2 \end{aligned} \tag{31}$$

where c is the vector of objective function coefficients, σ is the vector of unknown node stresses A_1 is the matrix of equality constraints derived from elements equilibrium, boundary conditions, and discontinuities equilibrium, b_1 is the corresponding right-hand vector of equality equations. A_2 is the matrix of inequality constraints derived from the yield criterion, and b_2 is the corresponding right-hand vector of inequality constraints.

5. Numerical examples

In this section, we select two classical examples from the tests published by Australian Association for Computer Aided Design (ACADS) to verify the method proposed in this paper. One slope is homogeneous and the other is a non-homogeneous slope.

To compare the accuracy of quadrilateral element versus triangular element, the slopes are meshed with a uniform element size varying from 1.0 to 2.5 m, and the number of sides in the linearized Mohr–Coulomb yield function is assumed 24 in all the following examples.
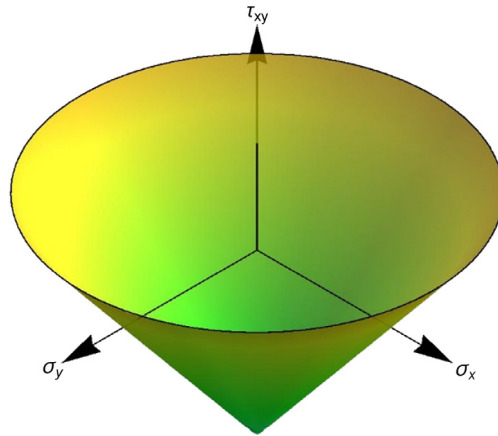
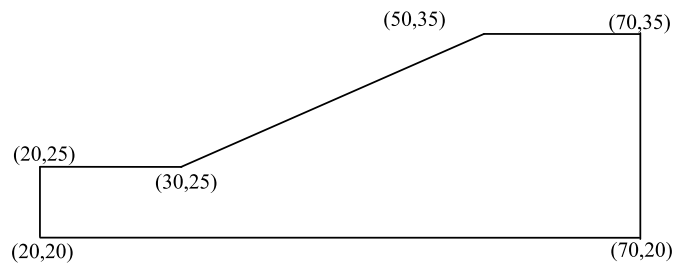**Fig. 3.** View of Mohr–Coulomb yield surface in $\sigma_x - \sigma_y - \tau_{xy}$ space.

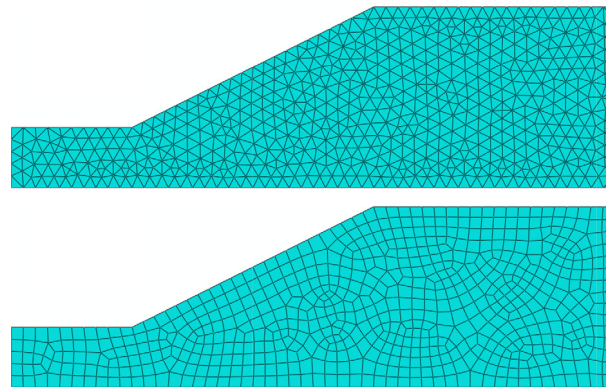**Fig. 4.** ACADS referenced slope example EX1(a). (Unit: m).

Fig. 5. Typical uniform mesh for homogeneous slope with element size is 1.0 m.

5.1. Homogeneous slope

The first example, named as Ex1(a), is a simple homogeneous slope, whose the geometry is shown in Fig. 4. The slope length and height are 20 m and 10 m, respectively. The material properties of the homogeneous slope are $\gamma = 20$ kN/m^3, $c = 3$ kPa, and $\varphi = 19.6°$. The accepted referee solution for the factor of safety is 1.00, thus the slope is at the point of failure.

The slope is meshed uniformly with global element size specified as 1.0 m, 1.5 m, 2.0 m, 2.5 m, respectively, and the typical mesh with element size is 1.0 m is shown in Fig. 5. By the way, the next example is also meshed uniformly with the same element sizes.

The lower bound of the safety factors with different element sizes are summarized in Table 1.

Fig. 6 depicts the safety factor–element size curves by using triangular element and quadrilateral element. As expected, the safety factor by using triangular element is lower than the one corresponding to quadrilateral element, and they are all less than the reference solution 1.0. Moreover, the results in Fig. 6 clearly indicate that safety factor by using quadrilateral element is more close to the reference solution than that by using triangular element (see Table 2).
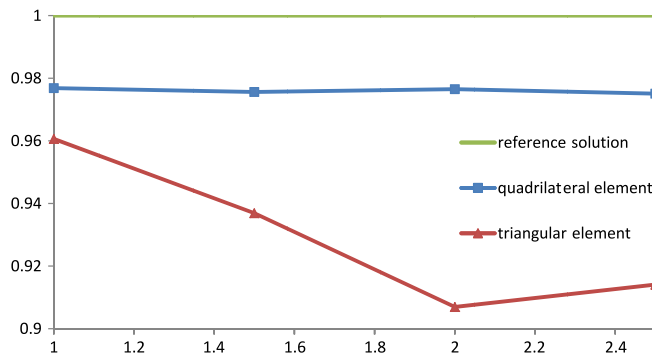
Fig. 6. A comparison of strength reduction factor between triangular element and quadrilateral element with different element sizes.
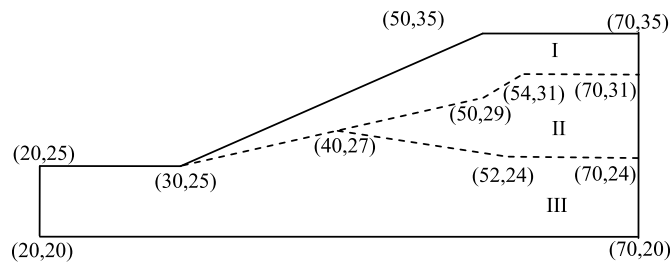

Fig. 7. ACADS referenced slope example EX1(c). (Unit: m).

Table 1
Strength reduction factor using triangular element and quadrilateral element with different element sizes.

Element size (m)	Triangular element	Quadrilateral element
2.5	0.9141	0.9751
2.0	0.9069	0.9765
1.5	0.9369	0.9756
1.0	0.9606	0.9768

Table 2
The material property of the nonhomogeneous slope.

No. of soil	c (kPa)	φ (°)	γ (kN/m^3)
I	0	38.0	19.5
II	5.3	23.0	19.5
II	7.2	20.0	19.5

5.2. Nonhomogeneous slope

Example 2, named as Ex1(c), is a study from ACADS of a non-homogeneous slope with three significantly different material parameters, whose property parameters are shown in Table 2. The geometry of the problem is shown in Fig. 7.

The recommended solution from ACADS (1989) is 1.359.

Table 3 and Fig. 8 show the comparison of safety factor obtained using triangular element and quadrilateral element for the nonhomogeneous slope. As can be seen from the table the safety factors using quadrilateral element are in relatively good agreement with the referee value on a coarse mesh. This can be explained by noting that the basis functions of triangular element are in the space of basis function of quadrilateral element, which leads to a higher accuracy of solution.

6. Conclusions

A lower bound analysis by using quadrilateral element is presented in this paper. The proposed approach is different from the method by using triangular element in that the equilibrium equation is no longer a linear equation. To linearize the equilibrium equation, the weak form of the equilibrium equations is performed, along with other equations, the finite element formulation of the lower bound method can be expressed as a linear programming. Two slope examples with homogeneous and nonhomogeneous materials have been solved in order to demonstrate the capabilities of the numerical

Table 3
Strength reduction factor using triangular element and quadrilateral element with different element sizes for the nonhomogeneous slope.

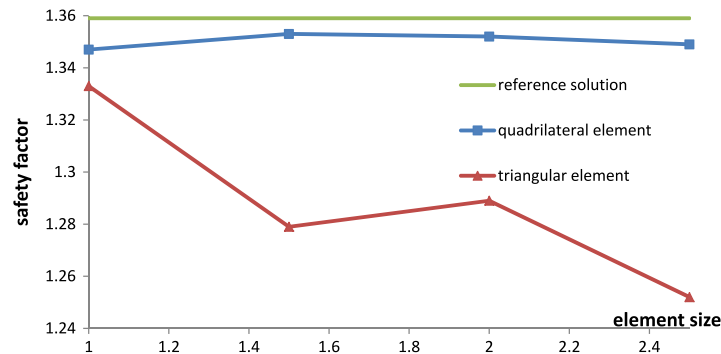| Element size (m)	Triangular element	Quadrilateral element
2.5	1.252	1.349
2.0	1.289	1.352
1.5	1.279	1.353
1.0	1.333	1.347

Fig. 8. A comparison of strength reduction factor between triangular element and quadrilateral element with different element sizes for the nonhomogeneous slope.

procedure. The obtained results are shown to be in good agreement with reference solution. The following remarks can be addressed as:

As expected, the safety factor by using quadrilateral element is more accurate than the one corresponding to triangular element when the element sizes are the same.

With the same element size, both the number of unknown variables and equations in the proposed method are less than that of triangular element method, that is to say, the scale of the proposed method is smaller than that of triangular element method.

Finally, it should be noted that the proposed method is not a rigorous method, since the weak form is used, but the result will converge to a stable state when the element size goes to zero.

References

[1] D.W. Wilson, et al., Undrained stability of a square tunnel where the shear strength increases linearly with depth, Comput. Geotech. (2012).
[2] S. Sloan, A. Assadi, Undrained stability of a square tunnel in a soil whose strength increases linearly with depth, Comput. Geotech. 12 (4) (1991) 321–346.
[3] J. Kim, J. Lee, Stability analysis of complex soil slopes using limit analysis, J. Geotech. Geoenviron. Eng. 128 (2002) 546.
[4] H.S. Yu, et al., Limit analysis versus limit equilibrium for slope stability, J. Geotech. Geoenviron. Eng. 124 (1) (1998) 1–11.
[5] J. Kumar, V.N. Khatri, Bearing capacity factors of circular foundations for a general c-phi soil using lower bound finite elements limit analysis, Int. J. Numer. Anal. Methods Geomech. 35 (3) (2011) 393–405.
[6] R. Salgado, et al., Two-and three-dimensional bearing capacity of foundations in clay, Geotechnique 54 (5) (2004) 297–306.
[7] V.N. Khatri, J. Kumar, Effect of anchor width on pullout capacity of strip anchors in sand, Can. Geotech. J. 48 (3) (2011) 511–517.
[8] R.S. Merifield, S.W. Sloan, The ultimate pullout capacity of anchors in frictional soils, Can. Geotech. J. 43 (8) (2006) 852–868.
[9] F.G. Degwitz, Numerical Upper and Lower Bound Limit Analysis for Braced Excavations, Massachusetts Institute of Technology, 2004.
[10] B. Ukritchon, A.J. Whittle, S.W. Sloan, Undrained stability of braced excavations in clay, J. Geotech. Geoenviron. Eng. 129 (8) (2003) 738–755.
[11] E. Christiansen, O.S. Pedersen, Automatic mesh refinement in limit analysis, Internat. J. Numer. Methods Engrg. 50 (6) (2001) 1331–1346.
[12] A.V. Lyamin, et al., Lower bound limit analysis with adaptive remeshing, Internat. J. Numer. Methods Engrg. 63 (14) (2005) 1961–1974.
[13] J. Munoz, et al., Upper and lower bounds in limit analysis: Adaptive meshing strategies and discontinuous loading, Internat. J. Numer. Methods Engrg. 77 (4) (2009) 471–501.
[14] S.W. Sloan, Lower bound limit analysis using finite-elements and linear-programming, Int. J. Numer. Anal. Methods Geomech. 12 (1) (1988) 61–77.